STRESS DROP ANALYSIS OF EARTHQUAKES IN THE VICINITY OF AYVACIK GEOTHERMAL RESERVOIR

by

Eda Yıldıran

B.S., Geophysical Engineering, Istanbul University, 2017

Submitted to Kandilli Observatory and Earthquake
Research Institute in partial fulfillment of
the requirements for the degree of
Master of Science

Graduate Program in Geophysics Department

Boğaziçi University

2023

ACKNOWLEDGEMENTS

I would like to thank my thesis advisor Assistant Prof.Dr Ali Özgün Konca of the Geophysics Department at Boğaziçi University. He has guided me during this thesis and I am gratefully indebted to his for his very valuable contribution on my thesis.

I would also like thank you Sezim Ezgi Güvercin for her invaluable support.

Finally, I would like to express my gratitude to my family aand my fiancee Habil Karaca for their patience and emotional supports.

ABSTRACT

STRESS DROP ANALYSIS OF EARTHQUAKES IN THE VICINITY OF AYVACIK GEOTHERMAL RESERVOIR

An earthquake swarm occurred in Çanakkale-Ayvacık, where started with an earthquake of M=5.4 magnitude on February 6, 2017, and more than 4000 earthquakes were recorded in 2 months. A significant number of these earthquakes were larger than $M_w = 4$. Most of the activity occurred on the southwest-dipping Tuzla Fault, which is a normal fault with WNW strike. Given that the fault region is a geothermal reservoir where active geothermal power plants operate, it is important to examine the characteristics of these earthquakes more closely. The activity started near a geothermal power plant and expanded along the Tuzla fault. In this thesis, the stress drops of earthquakes that occurred in the Ayvacık Region during the 2017 earthquake swarm was studied. Stress drop is a crucial macroscopic parameter for earthquakes and in geothermal regions, and variations in stress drop might indicate changes in stress conditions, especially pore pressure. The corner frequencies of 106 earthquakes with magnitudes greater than $M_L \geq 3.0$ were calculated from the P waveforms using 2 stations in the vicinity of the activity. We also calculated the moment magnitudes of 139 earthquakes with local magnitudes greater than 2.8 using P wave spectra. Our analysis shows that the stress drop of the earthquakes before and during the 2017 activity is quite variable. In addition, in comparison to the earthquakes that occurred before (~ 3 MPa), the average stress drop is higher with mean values of about $7 - 9$ MPa. We infer that the higher average stress drop during the 2017 activity might be related to a change in the pore pressure, where an increase in pore pressure might have led to a decrease in effective normal stress leading to higher slip values and therefore higher stress drops.

ÖZET

Ayvacık Jeotermal Rezervuarı civarındaki Depremlerin Stres Yitimi Analizi

6 Şubat 2017'de M=5.4 büyüklüğünde deprem ile başlayan Çanakkale-Ayvacık'ta bir deprem silsilesi meydana gelmiştir ve 2 ay içinde 4000'den fazla deprem kaydedilmiştir. Bu depremlerin önemli bir kısmının moment magnitüdü 4'ten büyüktür. Sismik aktivitenin çoğu, normal fay karakterinde olan güneybatı eğimli Tuzla Fayı üzerinde meydana gelmiştir. Bölgede aktif jeotermal enerji santrallerinin bulunması ve bir jeotermal rezervuar olması göz önüne alındığında, bu depremlerin özelliklerinin daha yakından incelenmesi önemlidir. Aktivite, bir jeotermal enerji santralinin yakınında başlamıştır ve Tuzla fayı yakın çevresinde yoğunlaşmıştır. Bu tezde, 2017 yılında Ayvacık bölgesinde meydana gelen depremlerin gerilme yitimleri incelenmiştir. Gerilme yitimi, depremler ve jeotermal bölgeler için önemli bir makroskopik parametredir ve gerilme yitimindeki değişiklikler özellikle gözenek basıncındaki bir değişiklikle oluşabileceği değerlendirilmektedir. Aktivite alanı yakınındaki 2 istasyon kullanılarak, $M_L > 3.0$ büyüklüğünde 106 depremin P dalga formlarından köşe frekansları hesaplanmıştır. Ayrıca, yerel magnitüdü 2.8'den büyük olan 139 P dalgası için moment magnitüdleri hesaplanmıştır. Bu çalışmada, 2017 aktivitesindeki depremlerin gerilme yitiminin oldukça değişken olduğu gösterilmektedir. Bununla birlikte, önceki depremlere ($\sim$ 3 MPa) kıyasla ortalama gerilme yitiminin yaklaşık $7 - 9$ MPa daha yüksek olduğunu gözlemledik. 2017 aktivitesi sırasındaki ortalama gerilme yitiminin yüksek olması, gözenek basıncındaki bir değişiklikle ilişkili olabilir. Gözenek basıncındaki artış, etkin normal stresin azalmasına ve dolayısıyla daha yüksek kayma değerlerine ve daha yüksek gerilme yitimlerine neden olduğu sonucuna ulaşılmıştır.

TABLE OF CONTENTS

LIST OF FIGURES

LIST OF TABLES

LIST OF SYMBOLS

c_0	P velocity at the source region
c_s	P velocity at the receiver region
D	The average offset on the fault
f	Frequency
f_c	Corner frequency
F_c	The average radiation coefficient of P wave
G_c	The geometrical spreading of P wave
S	the slip of the area
M_0	Seismic moment magnitude
m_b	Body wave magnitude
M_L	Local magnitude
$M_{\mathbf{w}}$	Moment magnitude
n	The high frequency fall of rate
Q	Quality factor
p	Pore pressure
t	Travel time
β	Shear wave velocity
γ	The sharpness of the transition between the flat and decreasing parts of the spectrum
μ	Rigidity
ρ_0	Density of the source zone
ρ_s	Density of the receiver zone
σ	Normal stress
$\triangle\sigma$	Stress drop
τ	Shear stress

Ω	Displacement amplitude spectrum
Ω_0	Long period displacement amplitude

LIST OF ACRONYMS/ABBREVIATIONS

AFAD	Afet ve Acil Durum Yönetim Başkanlığı
E	East
EZN	Ezine Station
KOERI	Kandilli Rasathanesi ve Deprem Araştırma Enstitüsü
KOCA	Koca Station
N	North
NAFZ	North Anatolian Fault Zone
S	South
SAC	Seismic Analysis Code
W	West

1. INTRODUCTION

Earthquakes occur due to the accumulation of stress along a fault plane. When the shear stress on a fault becomes higher than the yield strength, an earthquake occurs on a pre-existing crack. Following an earthquake, the stress decreases and gradually begins to accumulate again. Large earthquakes can alter the stress in surrounding areas based on the geometry of the fault, contributing to seismic activity [1].

Between January 14th–March 26th of 2017, more than 4000 earthquakes were recorded in the Tuzla, Ayvacık region of the city of Çanakkale in Northwestern Turkey [2]. Several studies addressed the tectonic implications of the 2017 earthquake sequence [2, 3]. Considering the unusual number of earthquakes and existence of geothermal power plants in operation, the 2017 sequence bears the question whether the stress perturbations cause by extraction and injection of fluids from the reservoir might have had any effects on the seismic activity in the region.

Geothermal plants can trigger fault movements due to increased pore pressure in underground rocks. This can lead to the initiation of micro-earthquakes in previously seismically inactive areas, and an increase in moderate earthquake activity in active areas [1]. For the 2017 Tuzla swarm, relocated seismicity shows that the seismic activity started at shallow depths close to the geothermal power plant, and propagated to further depths [4]. These results indicate that the geothermal reservoirs can alter the stress condition in fault zones and potentially create earthquake swarms.

In this thesis, we focused on the stress drops of earthquakes in the vicinity of the fault before, during and after the 2017 sequence. In Chapter 2, we provided a brief review of tectonic features of the Northwest Aegean region. Furthermore, we explore temporal evolution of seismic activity, examining earthquakes mechanism and proving detailed depth profiles in the Ayvacık region for the year 2017. In Chapter 3, we explain the selection of our data set derived from two stations from AFAD and KOERI. In

Chapter 4, we start by giving the details of the methodology on macroscopic parameters of earthquakes such has stress drop and seismic moment.In Chapter 5, we calculate the corner frequency from the P wave spectra and the seismic moment using the flat part of the spectra. We then calculate the stress drop of earthquakes. In Chapter 6, we interpret the implications of the results and In Chapter 7, finally conclude the thesis.

2. TECTONIC SETTING

Tuzla fault and the geothermal reservoir is located on the southwestern tip of the Biga Peninsula. Biga Peninsula is part of the shear zone that developed to the south of the North Anatolian Fault Zone (NAFZ). The NAFZ accommodates the relative motion of Anatolian Block microplate with respect to Eurasia. Another critical factor that shapes the active tectonics of the region is the extension in the Aegean due to rollback of the Hellenic slab.

Both northward movements of the Arabian and African plates and the westward motion of Anatolian block and the rollback of the Hellenic trench leading to wide scale extension, has shaped the tectonics of the region are seen in Figure 2.1 leading to various types of active faulting. The active faults are shown in the Figure 2.2 [2].

The backarc extension due to the rollback of the Hellenic subduction probably started in Middle Eocene ($\sim$ 45 Ma) but accelerated significantly and lead to a widespread extension and crustal thinning across the Aegean Extensional Province in Middle Miocene ($\sim$ 15 Ma) [5]. The crustal thinning and formation of the horst and graben systems led to high heat flow beneath the Aegean region [6].

The northwest Aegean region, forms a transition between the right-lateral dominant North Anatolian Fault Zone and the Aegean where E-W normal faults are dominant. As a result, transtensional features are dominant in the region. The active faults are normal faults, right-lateral strike-slip faults, extending in the NE-SW direction, while others are left-lateral strike-slip faults in the NW-SE direction [7]. The southern boundary of the Biga Peninsula region is bounded by the Edremit Gulf. The northern edge of the Edremit Gulf is bound by the Edremit Fault, which is a strike slip fault with significant normal component [3,8]. A distributed set of E - W, WSW right-lateral strike slip faults with some normal component also characterize the Biga Peninsula are shown in Figure 2.2.

2017 earthquake sequence occurred on the WNW trending Tuzla Fault. Tuzla fault is one of the series of WNW trending normal faults that developed in the south-western tip of Biga Peninsula, possibly due to differential motion of the strike-slip faults surrounding the area.

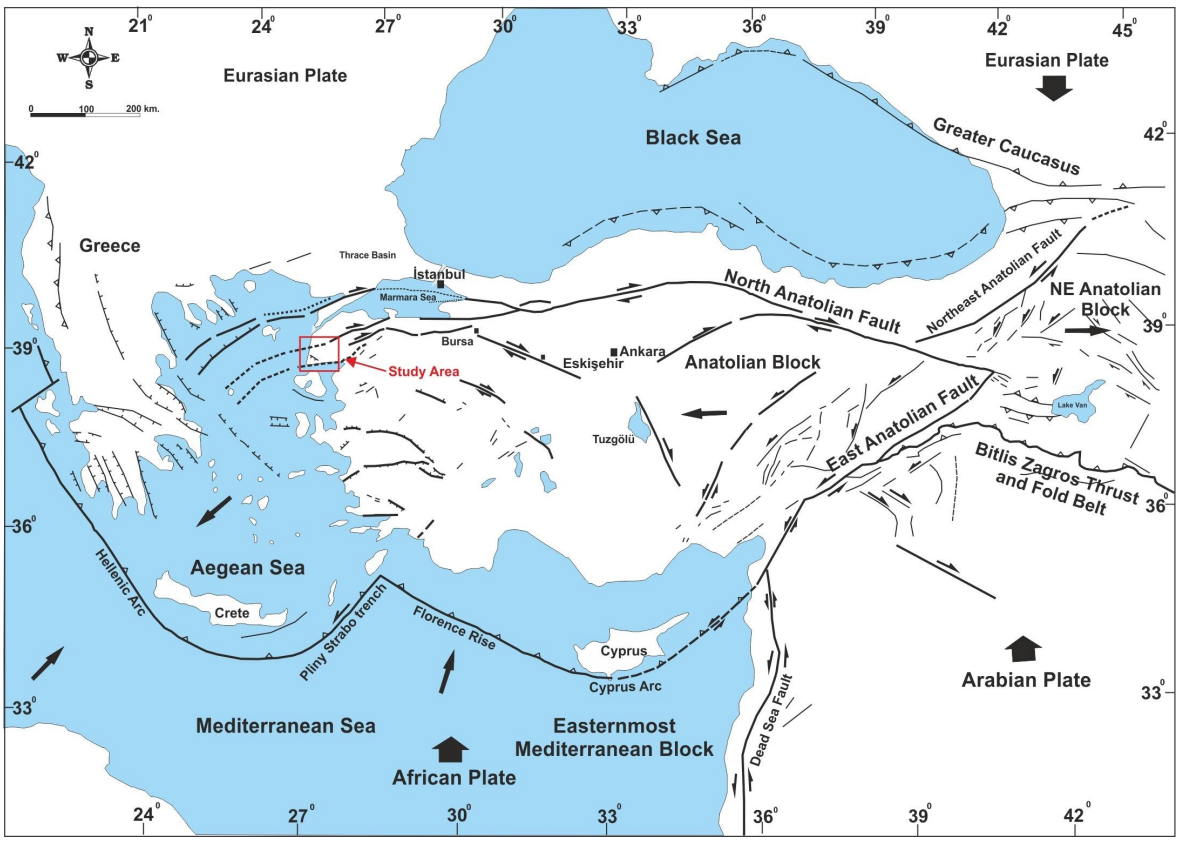

Figure 2.1. Study area with the tectonic framework of the Anatolian Block (Ozden et al, 2018) [2].

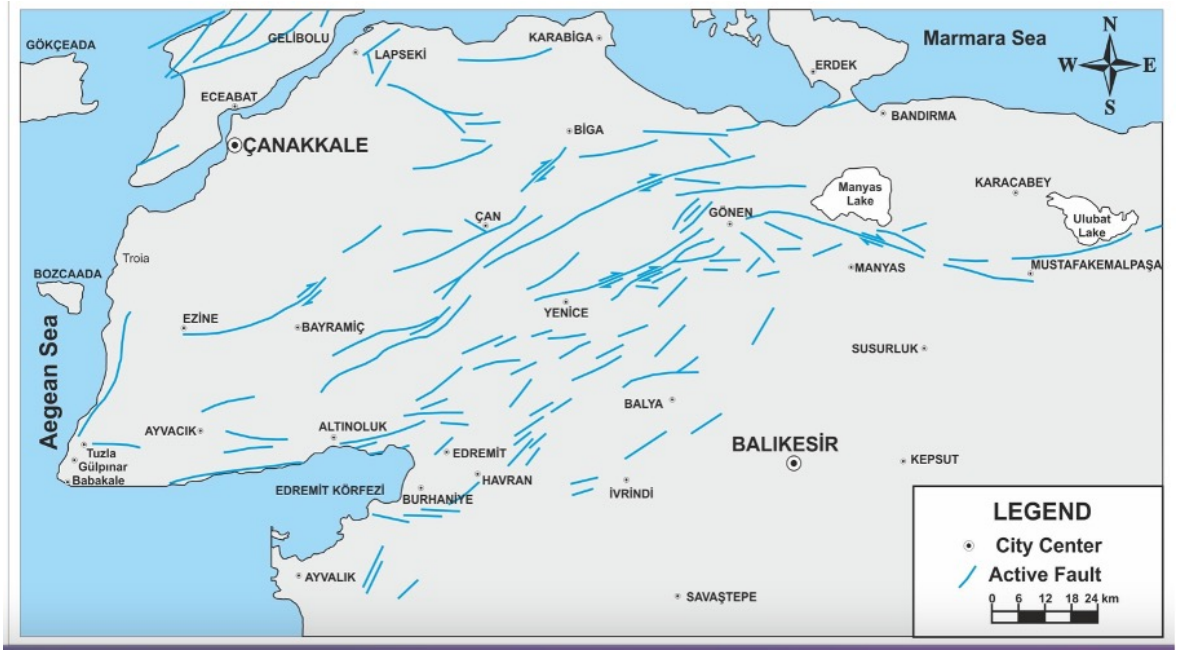

Figure 2.2. Active faults of Biga Peninsula (Ozden et al, 2018) [2]

2.1. DESCRIPTION OF THE 2017 EARTHQUAKE SWARM

Between January and March 2017 more than 4000 earthquake occurred along the southwestern tip of the Biga Peninsula, west of Ayvacık . Three of these earthquakes had magnitudes greater than 5. The largest earthquake in the sequence occurred on February 6, 2017 and had a magnitude of 5.3. The seismicity distribution clearly indicates that most of the earthquakes occurred along the southwest-dipping Tuzla Fault. In this study we utilized the relocated catalog of AFAD and KOERİ between 2015-2018 which consists of 6500 earthquakes are shown in Figure 2.3, [9].

In view of the fact that Ayvacık region is geothermal reservoir, it is a crucial evaluate these earthquakes more closely. When analyzing the temporal distribution of seismicity, it becomes obvious that the 2017 earthquake cluster initiated from a region near the active geothermal power plants and it propagated along the fault are seen in Figure 2.4. Prior to the 2017 swarm, seismic activity shows a scattered pattern, it became notably increased along the Tuzla Fault and significantly spread in two direction.

Focal mechanism of earthquakes larger than magnitude 4.0 obtained from regional waveforms using Cut and Paste method [10]. Fault mechanisms results are compatible with the WNW-ESE striking Tuzla Fault with normal mechanism are shown in Figure 2.5. The depths profiles also show a South dipping fault with a dip angle of $\sim 55^{\circ}$ are shown in Figure 2.6. The larger earthquakes reveal a listric character between the depths of $8-10$ km. The earthquakes are distributed along the fault over a length of $10-15$ km [9].

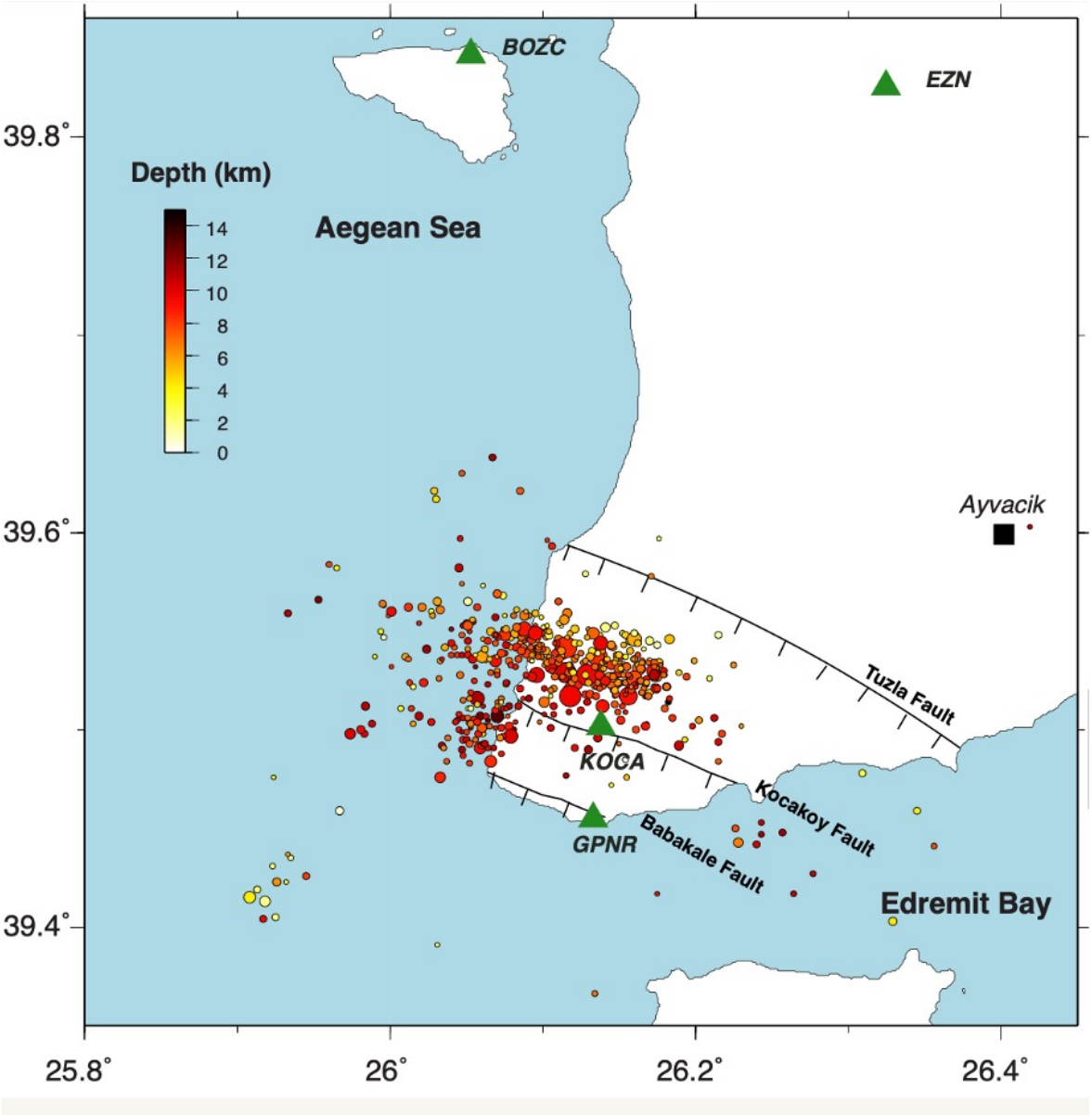

Figure 2.3. The normal faults located in the Western part of Ayvacık and the distribution of the 2017 earthquakes, colored according to their depths. Weak and strong ground motion stations in the region are indicated by green triangles (Konca et al, 2019), [9].

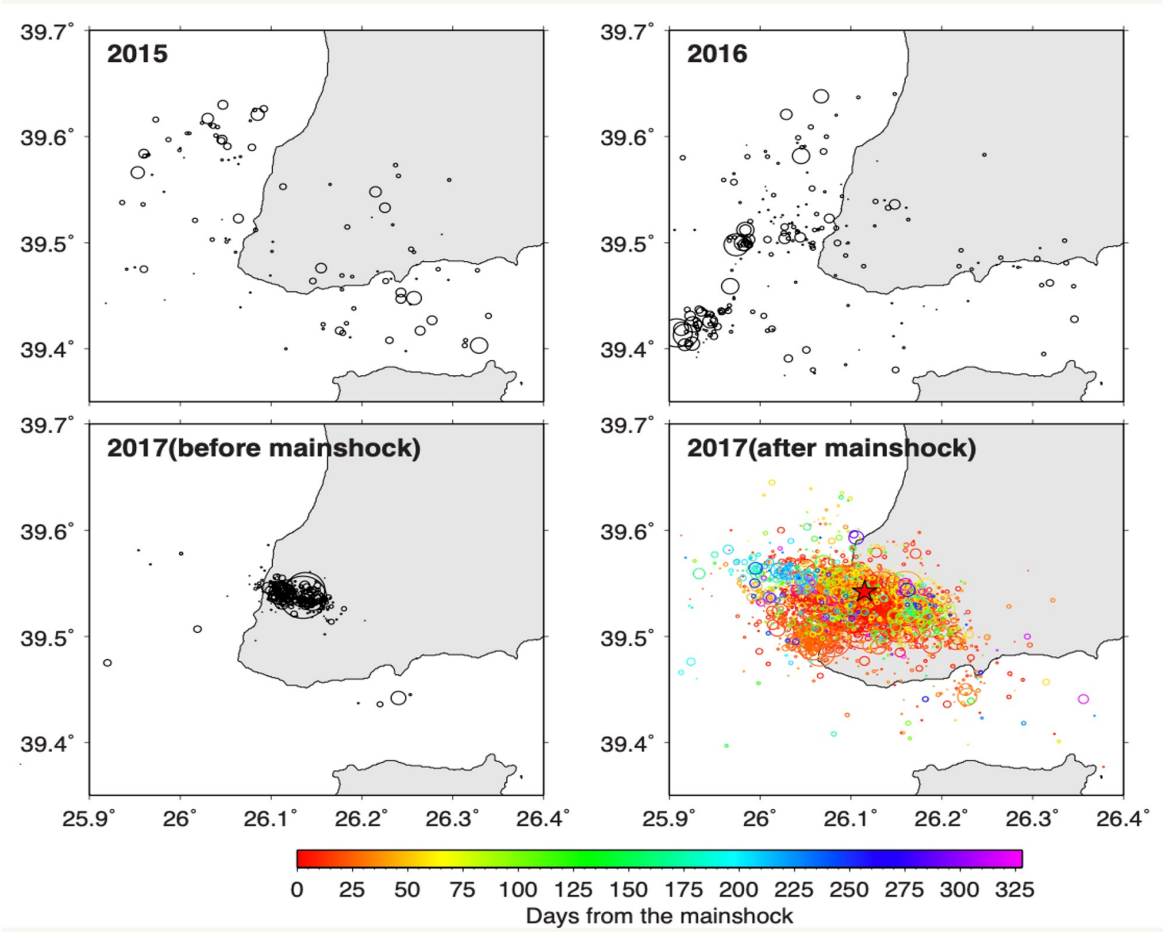

Figure 2.4. The distribution of seismicity prior to 2017 earthquakes and the temporal distribution of the earthquakes that occurred in 2017 (Konca et al,2019), [9].

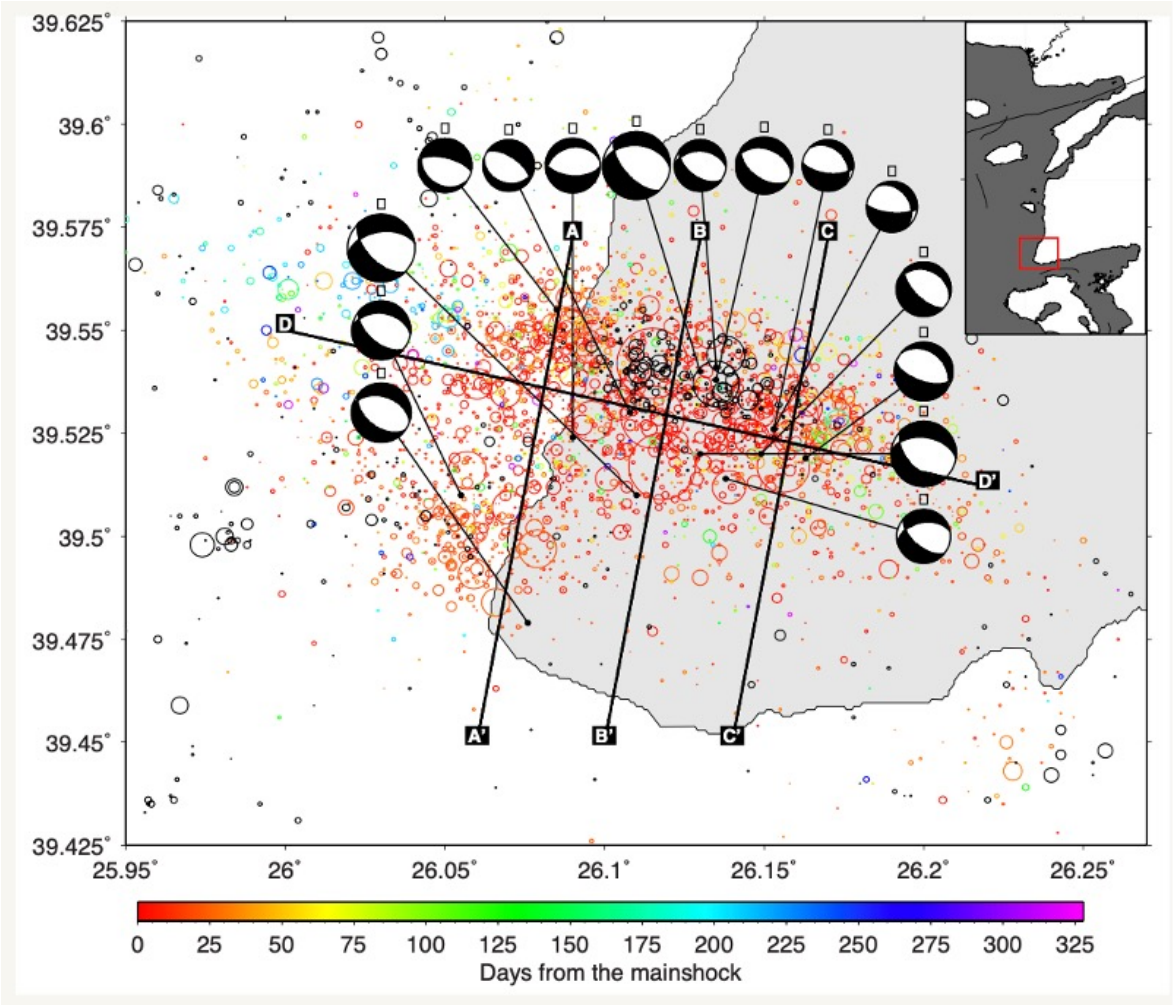

Figure 2.5. The temporal distribution of the 2017 earthquakes and the focal mechanism distribution of 15 selected earthquakes (Konca et al, 2019), [9].

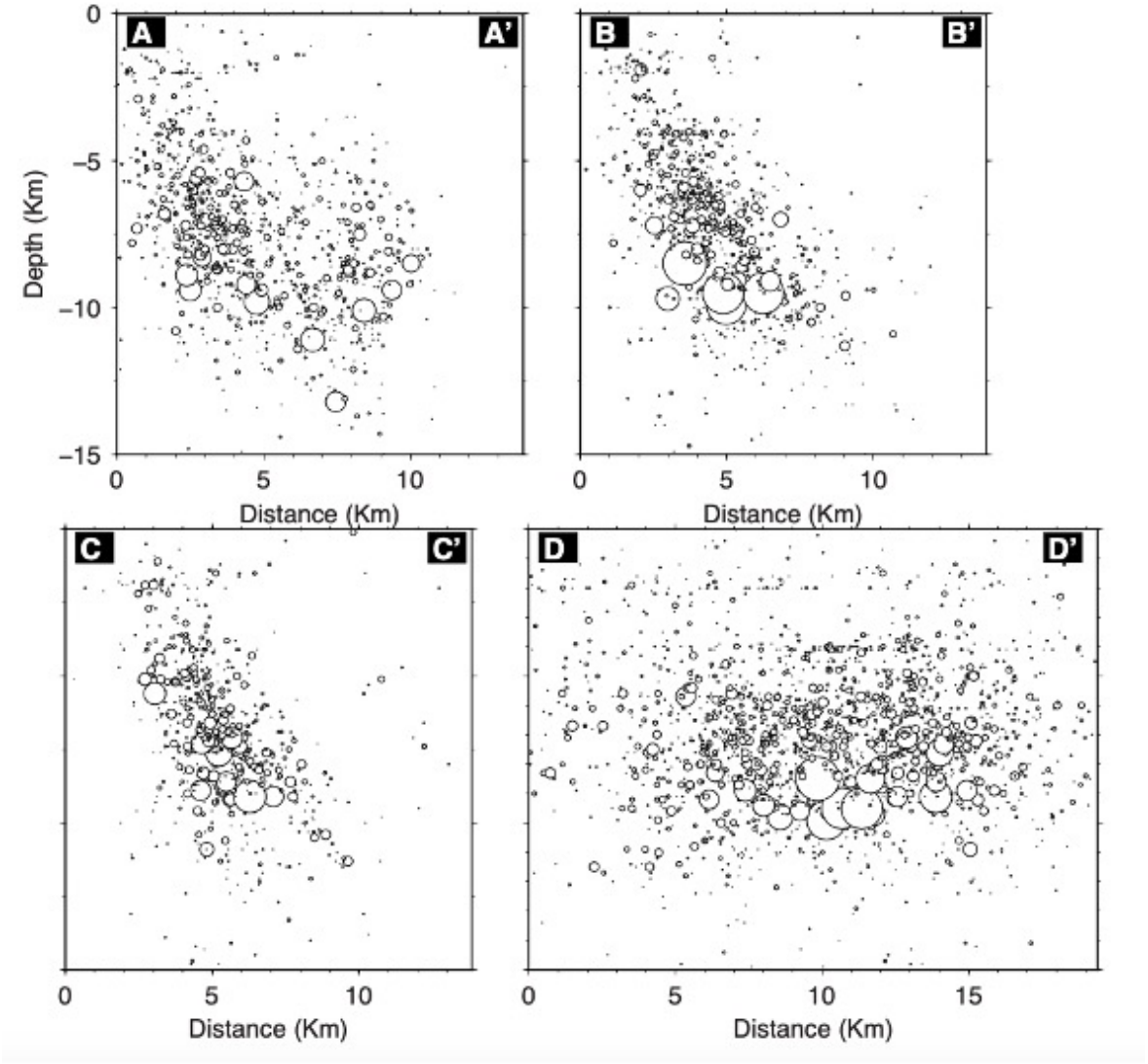

Figure 2.6. The distribution of earthquakes perpendicular to fault(A-C) and parallel(D) profiles , according to depth (Konca et al, 2019), [9].

3. DATA

In order to calculate the stress drop and moment magnitude of the 2017 Ayvacık earthquakes, 2 stations close to the earthquakes were utilized. One of the stations, EZN, is operated by Kandilli Observatory and Earthquakes Research Institute and the other station, KOCA, operated by AFAD. The station locations are shown in Figure 2.3. We converted waveforms to Seismic Analysis Code(SAC) format. To obtain displacement data, KOCA and EZN stations which are broadband stations were obtained by integral once.

To determine the stress drop and moment magnitude of the Ayvacık earthquakes in 2017, two stations, EZN and KOCA in close proximity to the earthquake epicenters were identified. The data was integrated to obtain displacement data from the broadband stations, KOCA and EZN.

For P wave spectra calculation, we used a vertical component in the analysis. P arrival times are manually picked. The displacement waveforms contain the direct P waves. Subsequently, the displacement amplitude spectra were obtained by performing a Fourier transform on them and examining the amplitude of the complex spectrum.

In this study, earthquakes with magnitudes equal to or greater than $M_L > 2.5$ were initially selected. The analysis focused on the vertical component to calculate the P-wave spectra. The P-wave arrival times were manually determined. The displacement waveforms captured the direct P waves. Subsequently, the Fourier transform was performed on these waveforms to obtain the displacement amplitude spectra. The amplitude of the complex function was examined during this process.

4. METHODS

In the classical method of modeling the earthquake source is described as a moment tensor or a distribution of moment tensors. Assuming the source region is small with respect to the receiver distance, and ignoring the higher frequencies related to source finiteness, the source can be represented as a point source. The mechanism of the earthquake is then represented by a single tensor called the moment tensor.

While the force couples associated with the moment tensor is determined by the magnitude, the geometry and the mechanism of the earthquake, the moment-time function determines how the moment is released in time. The far-field waves that propagate from the earthquake source is proportional to the derivative of the moment-time function. Generally, the direct far-field displacement pulse due to an earthquake source can be written as the convolution of two boxcar functions that are dependent on the displacement rise time and the rupture duration in time domain [11]. The rise time is the average duration of how long it takes on a point on the fault to rupture while the rupture time represents the propagation of rupture from the initiation point to the end of the rupture zone. The same expression in the frequency domain is in the form of the multiplication of two sinc functions.

If it is assumed that the rise and rupture times are the same, the displacement amplitude in the frequency(f) domain is expressed as a function that is flat and proportional to the seismic moment at low frequencies and decreases with a function of $1/f^2$ at high frequencies. The transition between the flat portion of the spectrum and $1/f^2$ decaying portion is characterized by the corner frequency, f_c.

The standard method of determining earthquake parameters, including magnitude, source size, and stress drop, is through frequency domain analysis of earthquake waveforms. This analysis involves fitting a displacement spectrum model using observed P and S wave spectra. In this study, the modified version of Brune's (1970) equation by Abercrombie (1995) was used to provide the displacement amplitude spectrum ,

$$\Omega(f) = \Omega_0 \frac{e^{-\pi f t/Q}}{[1 + (f/f_c)^{\gamma n}]^{1/\gamma}} \tag{4.1}$$

where f is the frequency, Ω_0 is the long period amplitude, f_c is the corner frequency, Q is the quality factor, t is the travel time between the station and the source, n is the high-frequency fall of rate and γ is the sharpness of the transition between the flat and decreasing parts of the spectrum [12, 13]. The most critical parameter is the corner frequency which determines the break frequency in the spectrum. The corner frequency is directly related to the radius of the ruptured area.

The seismic moment is defined as

$$M_0 = \mu S D \tag{4.2}$$

where μ is the rigidity, D is the average offset on the fault, and S is the area of fault [14, 15].

When the corner frequency and seismic moment are obtained, stress drop can be calculated using Equation 4.3 as

$$\triangle\sigma = \frac{7}{16}\left(\frac{f_c}{k\beta}\right)^3 M_0 \tag{4.3}$$

where β is shear wave velocity, k is 0.32 for P waves, f_c is the corner frequency and M_o is the seismic moment [16]. The magnitude of the low-frequency flat part in the body wave spectrum depends on parameters such as seismic moment, geometric propagation, and body wave velocity.

Earthquake occurs on preexisting cracks when the shear stress (τ) overcomes the normal stress (σ) times the frictional strength of the fault (μ). As the shear stress on a fault zone increases it becomes likely for a rupture to occur. Another way to initiate rupture is to decrease the normal stress. For earth problems effective normal stress needs to be considered, where the influence of pore pressure is taken into account. Amonton's Law [17] for friction is modified to include the influence of pore pressure. This equation is

$$\tau = \mu(\sigma - p) \tag{4.4}$$

where p is pore pressure, σ is the shear stress and μ is normal stress [1]. By increasing pore pressure, the effective normal stress decreases at high fluid pressure. Thus one can infer that an increase in pore pressure may lead to an increase in seismic activity.

In this study, we obtain both the corner frequency and seismic moment from the waveform spectra. The formulation proposed by Godano et al. (2015) was used to calculate the scalar seismic moment from the P-wave spectral amplitude [18],

$$M_0 = \frac{4\pi\sqrt{\rho_0\rho_s c_0 c_s}c_0^2\Omega_0}{F_c G_c} \tag{4.5}$$

where ρ_0 is the density of the source zone, ρ_s is the density of the receiver zone(respectively 2600 $kg \cdot m^{-3}$ and 2300 $kg \cdot m^{-3}$), c_0 is P wave velocity at the source region, c_s is P wave velocity at the receiver region(respectively 6100 m/s and 4800 m/s), F_c is the average radiation coefficient of P wave (0.52) and G_c is the geometrical spreading of P wave [19].

In order to calculate seismic moment, the corresponding Ω_0^P value is determined using the amplitude of the flat part of the spectrum of each station. Subsequently, the magnitude of the moment is calculated based on this value. To estimate the value of the seismic moment, the average of seismic moment values is taken from different stations, and the moment magnitude ($M_{\mathbf{w}}$) is obtained using the seismic moment magnitude (M_o) relationship.

5. RESULTS

5.1. Application to 2017 Ayvacık Earthquakes

5.1.1. Determination of Station-Specific Q Factor

In order to obtain source parameters such as corner frequency and spectral amplitude, it is crucial to correct the path effects. Specifically, the estimation of the corner frequency is strongly dependent on the accurate correction of the attenuation (Equation 4.1). Attenuation is often characterized using the seismic quality factor (Q). The quality factor is a measure of the number of cycles required for the amplitude to decay to $1/e$ of the original value. Since the number of cycles for a source-station path depends on the frequency of the body waves, the correction and the choice of the Q value significantly change the amplitude spectrum and the estimation of the corner frequency. Choosing the right Q value is especially crucial when we derive the corner frequency, and thereby the stress drop, from the spectrum analysis [20, 21].

An average quality factor value was determined for the P waves at each station using the average attenuation curves of earthquakes. A single quality factor (Q) value was used for each station. For the P wave, $Q = 150$ was used for the KOCA station, while $Q = 350$ was used for the EZN station. The spectral decay of various earthquakes and spectral decay of modified Brune model using the best fitting quality factor (Q) value at KOCA station as shown in Figure 5.1.

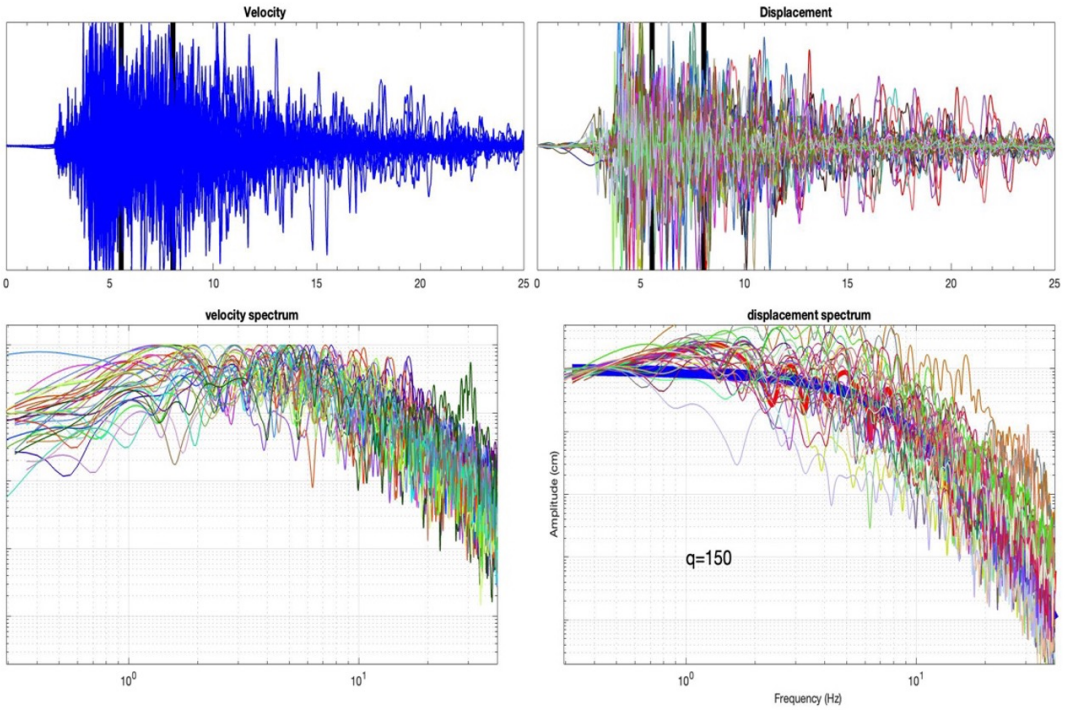

Figure 5.1. Velocity and displacement and waveforms (top) and normalized spectra (bottom) of earthquakes that occurred in the Tuzla region recorded at KOCA station. The thick blue spectrum curve indicates a modified Brune spectrum with a corner frequency of 5 Hz and a quality factor of 150.

As seen in Figure 5.1, the normalized spectra of earthquakes with varying magnitudes and different corner frequencies indicate similar falloff curves at high frequencies. For each earthquake, the most compatible corner frequencies were determined according to the fit of the normalized Brune amplitude spectrum to the data. As seen in Figure 5.1 demonstrates that the average attenuation coefficient of source-station pairs with similar locations is very close to each other.

5.1.2. Determination of Corner Frequency

To determine the best-fit corner frequency, a displacement spectrum model was fitted to the observed P-wave spectrum. Generally, the far-field displacement formula has been selected $\gamma = 1$, $n = 2$ parameters in Equation 4.1 by proposed Brune 1970 [12].

In the study, two stations (KOCA and EZN) were used for the calculation of P-wave corner frequency. For each earthquake, the most compatible corner frequencies were determined according to the fit of the normalized Brune amplitude spectrum to the data using a grid search. Corner frequencies were determined for a total of 106 earthquakes using P waves. Moment magnitudes were calculated for 139 earthquakes with $M_L > 2.8$ from the P wave spectra. Examples of waveforms, amplitude spectra, and best-fitting model results for some of the earthquakes that occurred in 2016 and 2017 are shown in Figures 5.2 and in Figures 5.3. The P corner frequencies were determined by taking the logarithmic mean of the corner frequency values obtained from different stations for each earthquake. Table 1 displays the corner frequency values.

Figure 5.5 shows the relationship between earthquakes, their local magnitudes, and corner frequencies. Although significant variations were observed in corner frequencies of earthquakes with similar magnitudes, they generally appear consistent with earthquake magnitude relationships.

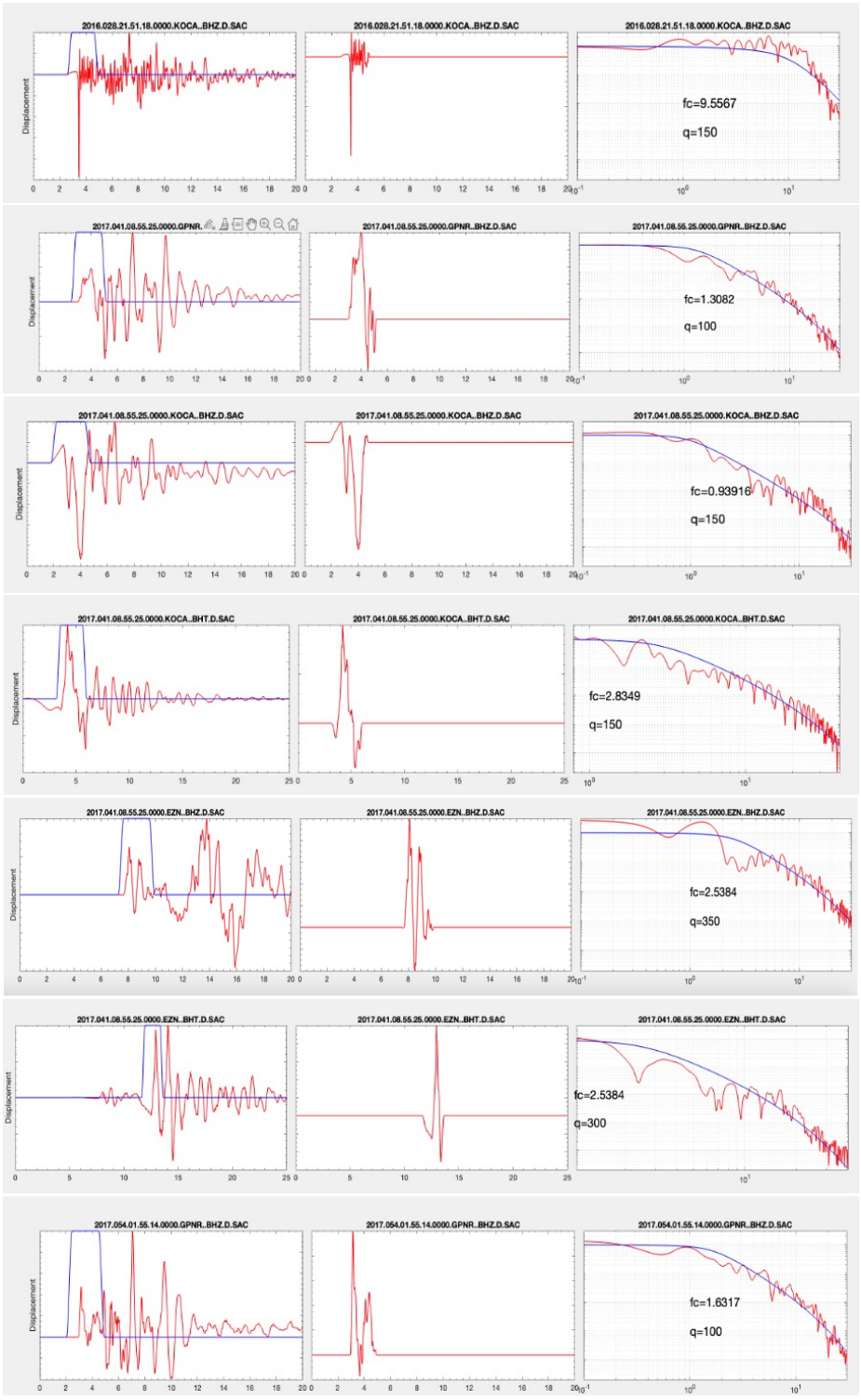

Figure 5.2. Displacement waveforms for the P wave(left) and waveforms used for the frame are shown(blue). The names of the earthquake records are specified above. Framed P waveforms (middle). The spectrum of the P wave(red) with best fitting Brune spectra (right).

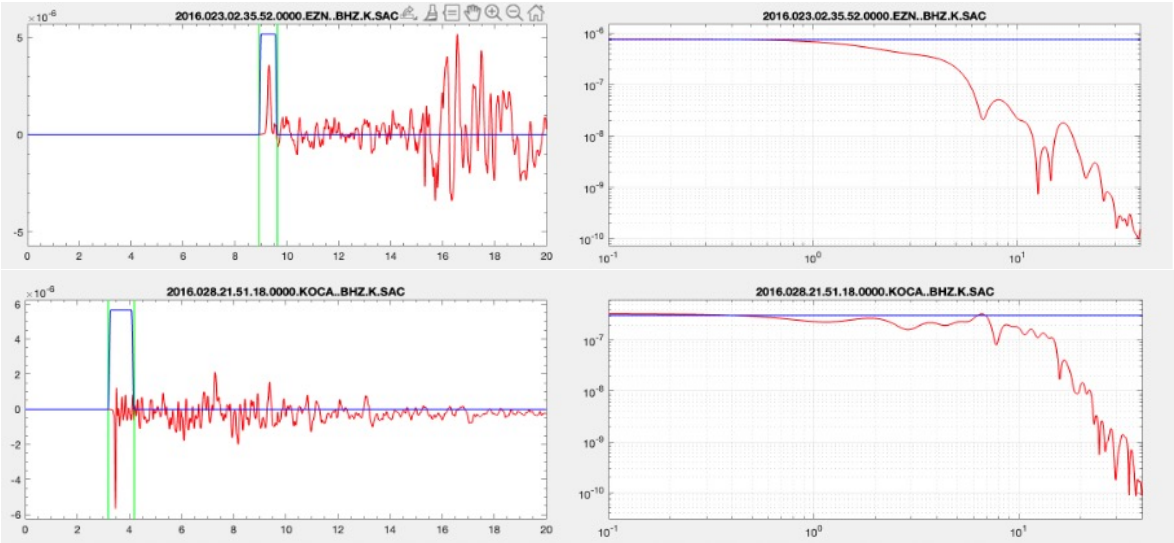

Figure 5.3. Displacement waveforms for the P wave(left) and waveforms used for the frame are shown(blue). The names of the earthquake records are specified above. The spectrum of the P wave(red) with best fitting Brune spectra(right).

5.1.3. Calculation of Moment Magnitude

The corner frequency of earthquakes provides information about the duration and length of fault rupture. The flat portion of the spectrum at frequencies lower than the corner frequency is utilized for calculating the moment magnitude of earthquakes. In this study, after calculating the corner frequencies, the moment magnitude of earthquakes was calculated using the region where the spectrum is flat. After calculating the moment magnitude values of each earthquake at different stations, the averages were taken to determine the moment magnitude from the P waveforms. The calculation of the scaler seismic moment from the P wave spectrum in Equation 4.5 is based on the formulation proposed by Godana et al. [18].

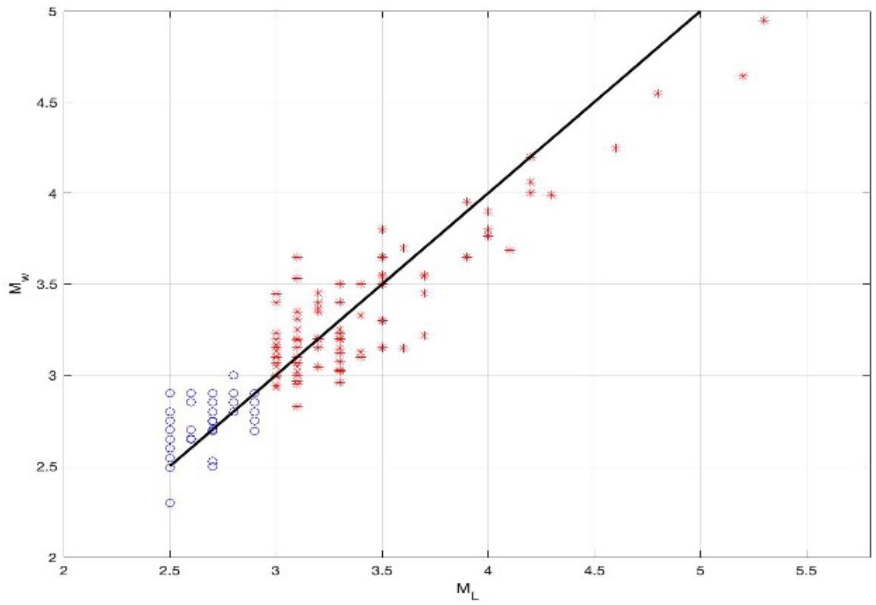

Figure 5.4. Comparison of local magnitudes and moment magnitudes obtained from P waves. The thick black line indicates the case where both the equal.

As shown in Figure 5.4, Comparison of the moment magnitude calculated in this study with local magnitude calculated by AFAD. This comparison generally shows a good fit, but there is some scattering. On the other hand, it has been observed that local magnitudes are systematically larger than moment magnitudes, especially for earthquakes larger than 4.

5.1.4. Calculation of Stress drops

Following the determination of the corner frequency of each earthquake, the seismic moment of each earthquake was calculated using the flat portion of the spectrum as described in Equation 4.3. Using the amplitude of the flat portion of the displacement spectrum, the moment magnitude ($M_{\mathbf{w}}$) values for each earthquake at various stations were computed, and the average of these values was utilized to determine the moment magnitude.

In Figure 5.5 illustrates the variations in stress drop over time. During the 2017 activity, significantly high-stress drop earthquakes are observed. The geographical distribution of stress drops is presented in Figure 5.6. Furthermore, in Figure 5.7 illustrates the stress drop in relation to distance and time from the geothermal reservoir (2016-2017). In Figure 5.8 displays the stress drop based on the distance from the geothermal area for the year 2017 activity.

The distributions shown in Figures 5.7 and Figures 5.8 indicate a significant number of larger magnitude earthquakes with substantial stress drop in close proximity to the geothermal energy region. However, it is noteworthy that the distribution appears to be quite scattered. In Figure 5.7 also shows that the activity started close to the geothermal power plant and spread to the Tuzla fault.

In Figure 5.8 shows the average distribution of stress drop over different time intervals. In addition, the seismic activity in the Ayvacık region has been computed as the daily seismicity rate. The seismicity catalog was obtained by combining data from AFAD and KOERI data base.

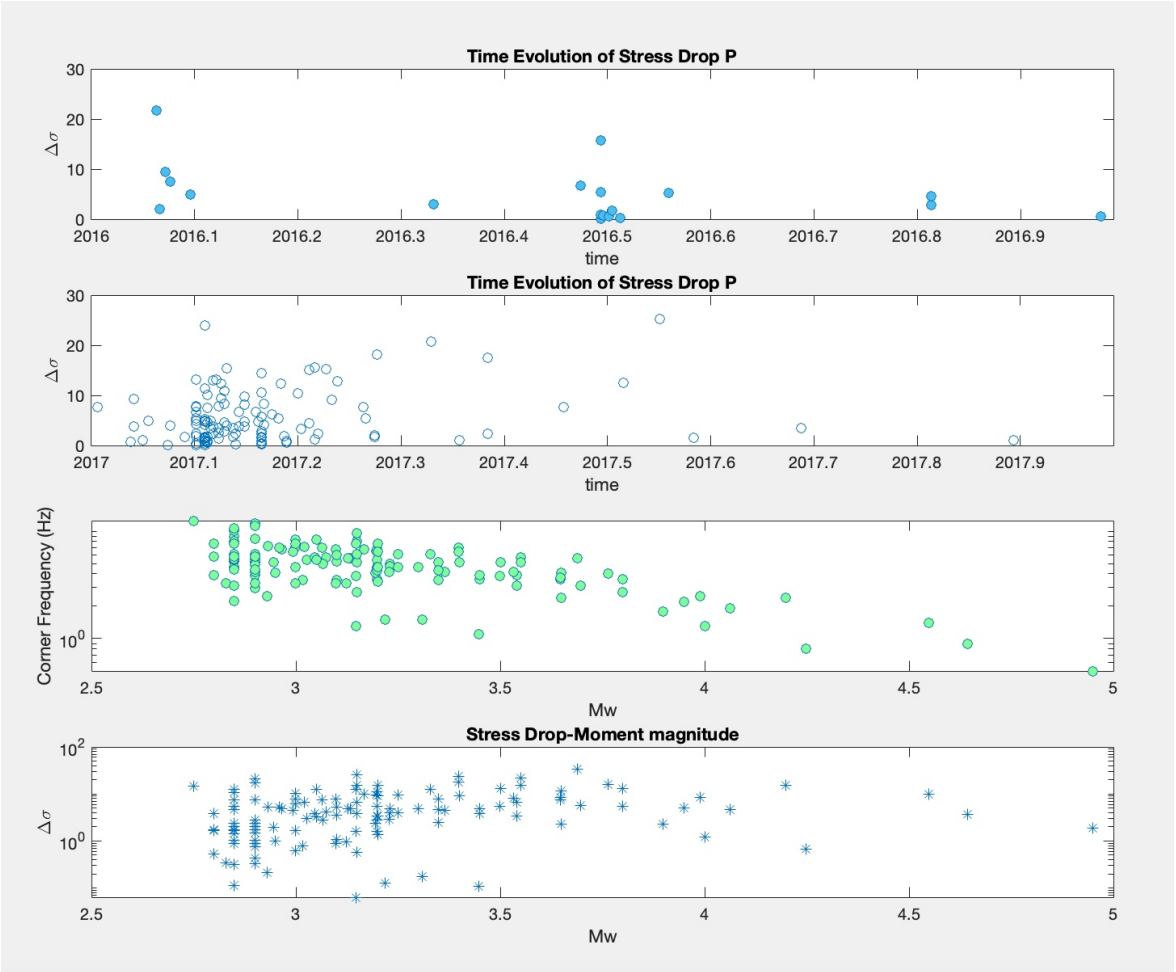

Figure 5.5. Temporal distribution of stress drop of earthquakes that occurred in 2016 in Tuzla region, (b) Temporal distribution of stress drop of earthquakes that occurred in 2017 in Tuzla region, (c)Relationship between moment magnitude and corner frequency, (d)Relationship between stress drop and moment magnitude.

In Figure 5.5(d) relationship between stress drop and moment magnitude is explored. The values of earthquakes with magnitudes 2.8 and below were excluded from the analysis due to the high attenuation observed in these earthquakes, which may lead to an overestimation of the corner frequency. Therefore, only earthquakes with a magnitude greater than 2.8 ($M_{\mathbf{w}} > 2.8$) were included in the analysis.

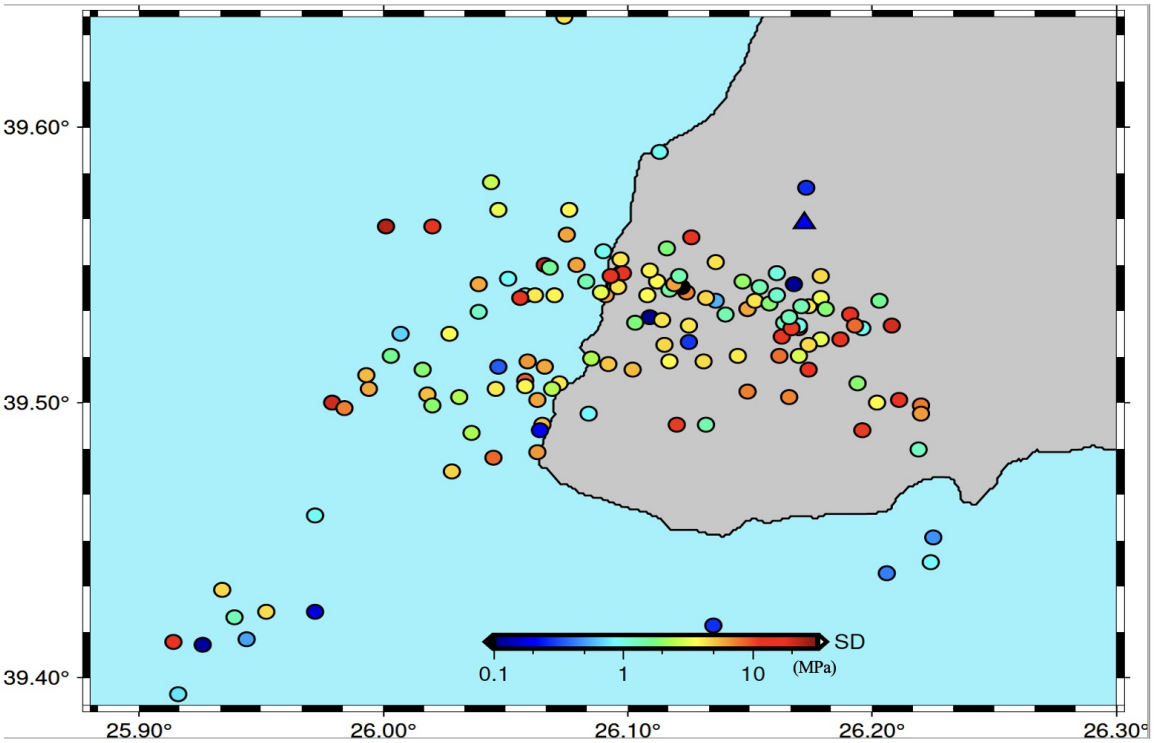

Figure 5.6. The distribution of stress drops of earthquakes in 2017 Ayvacık earthquakes(given in MPa).The region indicated by triangle shows the location of the geothermal power plant facility.

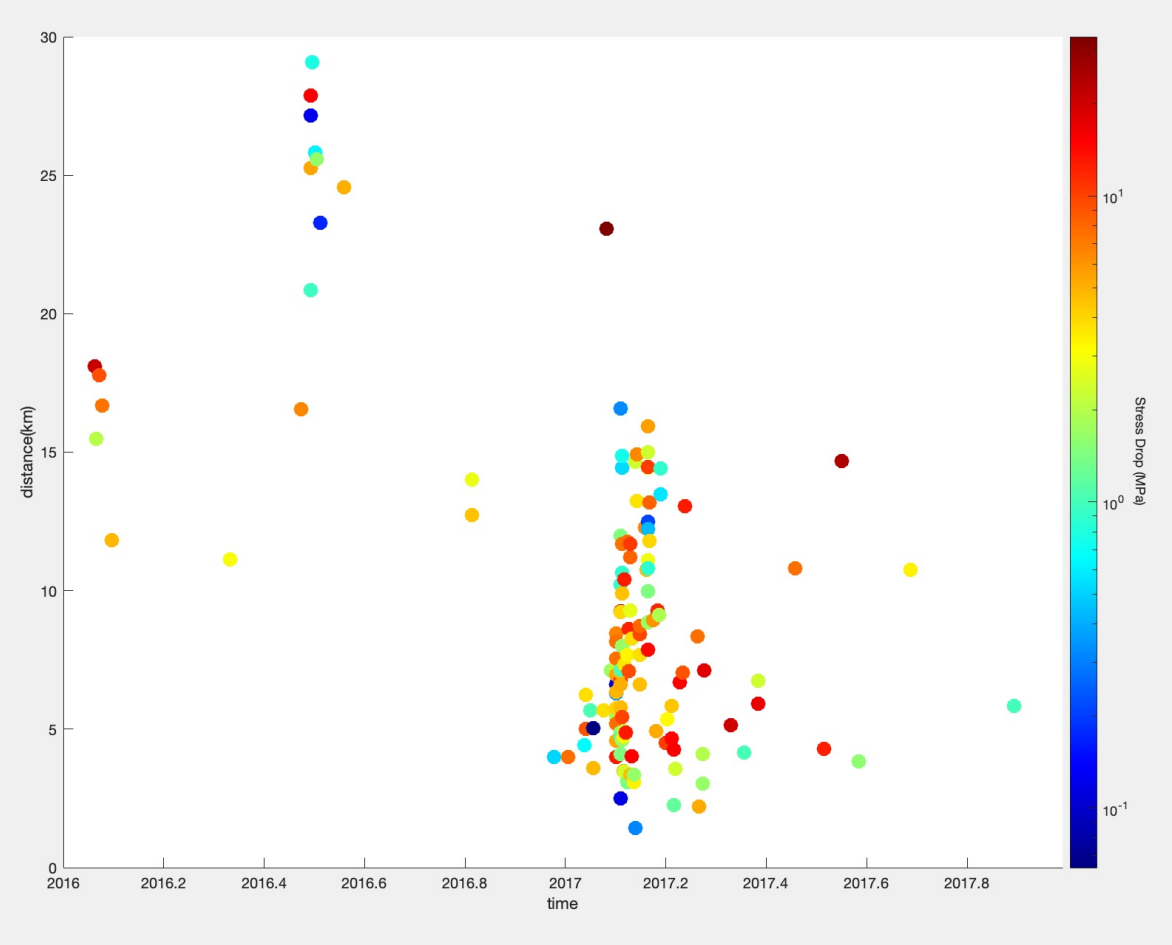

Figure 5.7. The stress drops of earthquakes that occurred during the period of 2016-2017 are represented based on their distance from geothermal power plants and time. The stress drops are shown logarithmic scale and measured in MPa units.

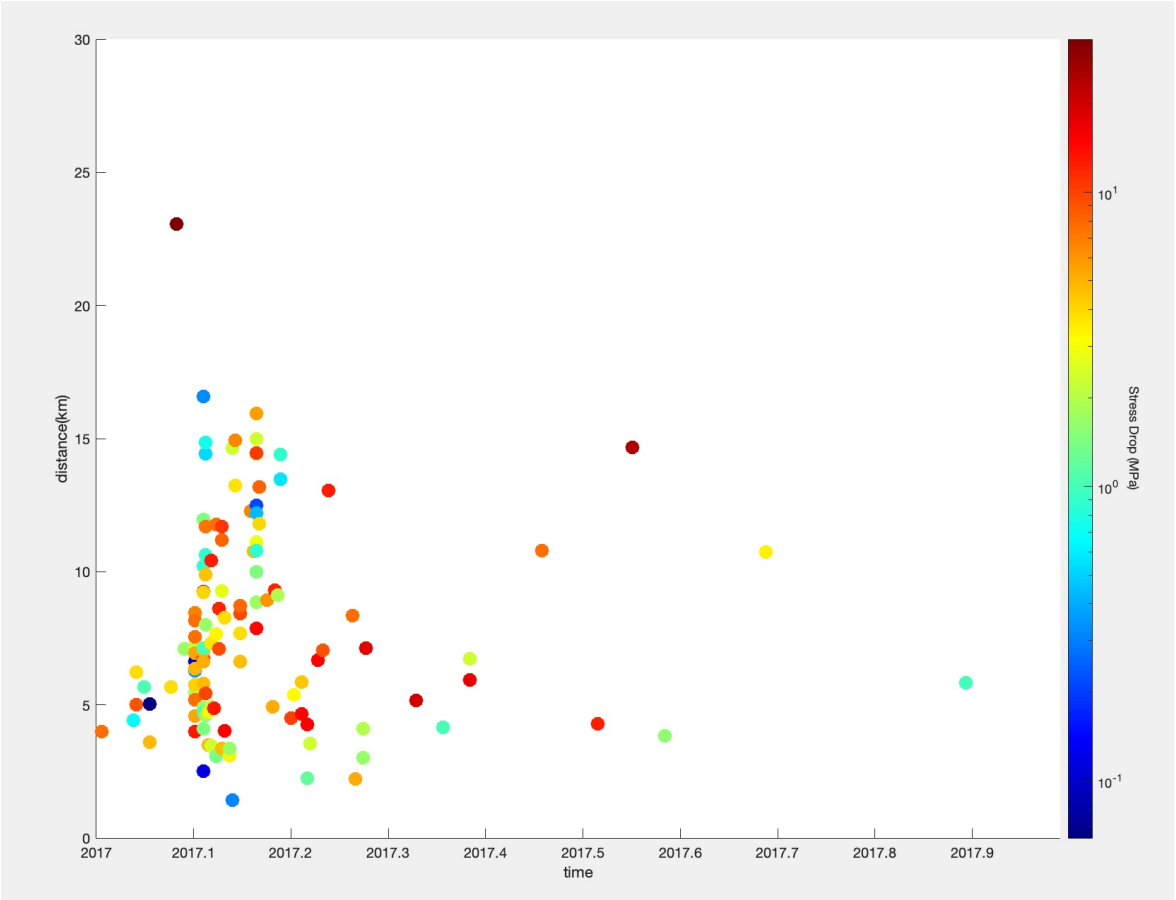

Figure 5.8. The stress drops of earthquakes that occurred during the period of 2017 are represented based on their distance from geothermal power plants and time. The stress drops are shown logarithmic scale and measured in MPa units.

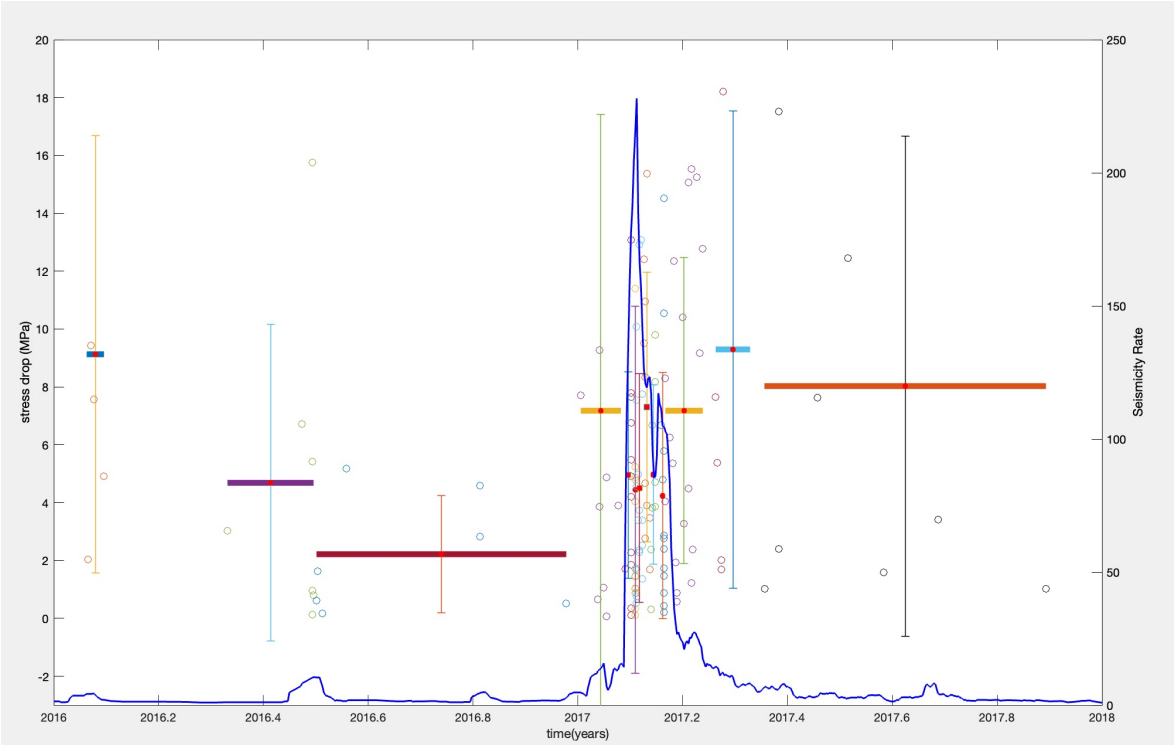

Figure 5.9. Seismicity rate (blue curve) and temporal evolution of the mean stress drop. The horizontal lines show the average stress drop values of earthquakes within the time interval(left axis). Uncertainty bars represent $1-\sigma$ standard deviations from the mean values. The seismicity distribution was calculated on a daily basis with 5 days weighted averages (right axis).

Prior to the seismic activity in 2017, the average stress drops showed a declining trend. In the second half of the year 2016, the average stress drop is about 3 MPa. However, with the onset of the seismic activity in January 2017, the stress drops increased significantly. Typically the stress drop values of earthquakes range between 1 and 10 MPa, as reported by Abercrombie and Rice [22]. The investigation of stress drop values in the Ayvacık region indicated that they fell within the normal range. Nevertheless, during the onset of the seismic activity between 2016 and 2017, the average stress drop values were very close to 10 MPa, close to the upper limit of the normal range. At the beginning of 2016, the fewer earthquakes and lower seismic activity levels may have resulted in less conclusive average stress drop values.

During the 2017 activity, the elevated stress drop values in the geothermal area can be attributed to changes in pore pressure. The pore pressure alterations lead to a decrease in effective normal stress, consequently leading to a higher shear slip and therefore higher stress drop.

6. DISCUSSION

The stress drop values of earthquakes in the Tuzla-Ayvacik region obtained in this study range from 0.06 MPa to the highest value of 33.16 MPa. The 2017 swarm is also associated with relatively high values of stress drops with a mean value around 7-9 MPa.

Allmann and Shearer studied 2000 earthquake with $m_b \geq 5.5$ in Japan [23]. They found earthquakes with stress drop values between 0.3 and 50 MPa. The median of the stress drop values is 4 Mpa and is independent of magnitude. According to Baltay the mean stress drop and apparent stress does not show significant variation except some anomalous activities [24] . Considering the median value of 4 MPa and mean values of 7-9 MPa during the 2017 earthquake swarm in Ayvacık, it is clear that on average the anomalous activity has high stress drop.

Eyidoğan argues that since the geothermal power plant production began in 2012, the seismic activity in Ayvacık region has been increasing and larger magnitude earthquakes started occurring with increasing geothermal power plant activity. He argues that the extraction and reinjection of fluids changes the stress environment leading to earthquakes along the Tuzla Fault [25] .

On the other hand, it is challenging to relate the geothermal power plant activity to seismicity. The relocated hypocenter locations of the 2017 activity clearly indicate a listric dipping fault structure consistent with the normal focal mechanisms. The depth range of earthquakes vary from vary several km to 15 km. Considering that the geothermal power plants operate in the top several km, direct correlation of earthquakes at 10-15 km depth with the extraction and injection of fluids requires further research. However, observations that the activity started near the geothermal reservoir and at shallow depths might be an indication that the geothermal activity might have triggered the 2017 swarm.

Staszek studied the Geysers Geothermal Field in California. He find that the high stress drop earthquakes occur when injection rate starts to decrease [26]. Nikurashin and Kwiatek carried out that a decrease in stress drop associated with higher pore fluid pressure during geothermal injection in Switzerland. These examples show that while changes in stress drop are observed, relation to the injection rates are not straight forward [27], [28].

In the case of Tuzla activity, since we do not have access to extraction and injection rates, a direct comparison can not be made. However, considering that the geothermal power plant is close to the normal fault, where the largest stress orientation σ_1 is vertical, and the activity started near the operation site, it is viable that small changes in stress conditions, such as fluid extraction and injection, changes in pore pressure leading to anomalous seismic activity.

Gezer found a correlation between the locations of geothermal fields and the b-value parameter. The spatiotemporal analysis of earthquake data along the Saros-Ayvacık-Edremit reveals an increase in b-values prior to the 2014 and 2017 earthquakes, followed by a subsequent decline, signifying distinct seismic behavior during these events [29] .

7. CONCLUSION

In this study, we examined the activity along the Tuzla Fault in the Ayvacık region of Çanakkale before, during, and after the seismic crisis of 2017. Considering that the region is characterized by a geothermal reservoir that is actively exploited by geothermal power plants, it is important to understand the source characteristics of the earthquakes during this unusual activity.

In that regard, we study the stress of drops of earthquakes in the region. Our results show that the stress drop values for earthquakes before the 2017 activity are relatively low with values around 1 MPa. The stress drop values during the high rate of activity during the first 2 months of 2017 are highly variable, but on average are relatively high about 8 MPa. The mean stress drop in the region before the earthquake is about 3 MPa. This rapid increase of stress drop values might be related to the pore pressure changes. Whether the shallow geothermal activity of extracting and injecting ground water leads to earthquakes at the depths of 10-15 km requires further research.

REFERENCES

1. Kanamori, H. and E. E. Brodsky, "The Physics of Earthquakes", *Physics today*, Vol. 54, No. 6, pp. 34–40, 2001.

2. Özden, S., S. Över, S. A. Poyraz, Y. Güneş and A. Pınar, "Tectonic Implications of The 2017 Ayvacık (Çanakkale) Earthquakes, Biga Peninsula, NW Turkey", *Journal of Asian Earth Sciences*, Vol. 154, pp. 125–141, 2018.

3. Koçyiğit, A. and Ş. Gürboğa, "Active tectonics of Gülpınar-Tuzla area (Biga Peninsula, NW Turkey): The Source of 6 February-24 March 2017 Earthquake Cluster", *Bulletin of the Mineral Research and Exploration*, Vol. 166, No. 166, pp. 85–112, 2021.

4. Bulut, F., E. Havazlı, C. Yaltırak, A. Doğru, A. Sabuncu and H. Özener, "The 2017 Ayvacık Earthquake Sequence: A Listric Fault Activated Beneath Tuzla/Çanakkale Geothermal Reservoir (Western Turkey)", *Proceedings of 43rd Workshop on Geothermal Reservoir Engineering Stanford University*, 2018.

5. Brun, J.-P., C. Faccenna, F. Gueydan, D. Sokoutis, M. Philippon, K. Kydonakis and C. Gorini, "The Two-Stage Aegean Extension, from ,Localized to Distributed, A Result of Slab Rollback Acceleration", *Canadian journal of earth sciences*, Vol. 53, No. 11, pp. 1142–1157, 2016.

6. Uğur, A., E. U. Ulugergerli and S. Kutlu, "The Assessment of Geothermal Potential of Turkey by means of Heat Low Estimation", *Bulletin of the Mineral Research and Exploration*, Vol. 149, No. 149, pp. 201–210, 2014.

7. Demirel, Z., T. Yildirim and M. Burçak, "Preliminary Study on the Occurrence of Geothermal Systems in the Tectonic Compressional Regions: An Example from The Derman Geothermal Field in the Biga Peninsula, Turkey", *Journal of Asian*

Earth Sciences, Vol. 22, No. 5, pp. 495–501, 2004.

8. Altınok, Y., "6 Ekim 1944 Edremit Körfezi-Ayvacık Depreminin Makrosismik Değerlendirilmesi", *İstanbul Yerbilimleri Dergisi*, Vol. 25, No. 1, pp. 41–53, 2013.

9. Konca, A. O., S. E. Güvercin, H. Karabulut, F. Turhan and T. Bekler, "Analysis of an Unusual Seismic Activity of a Geothermal Reservoir in Ayvacık, Çanakkale, Northwestern Turkey.", *Geophysical Research Abstracts*, Vol. 21, 2019.

10. Zhu, L. and D. V. Helmberger, "Advancement in Source Estimation Techniques Using Broadband Regional Seismograms", *Bulletin of the Seismological Society of America*, Vol. 86, No. 5, pp. 1634–1641, 1996.

11. Haskell, N., "Total Energy and Energy Spectral Density of Elastic Wave Radiation from Propagating Faults", *Bulletin of the Seismological Society of America*, Vol. 54, No. 6A, pp. 1811–1841, 1964.

12. Brune, J. N., "Tectonic Stress and the Spectra of Seismic Shear Waves from Earthquakes", *Journal of geophysical research*, Vol. 75, No. 26, pp. 4997–5009, 1970.

13. Abercrombie, R. E., "Earthquake Source Scaling Relationships from -1 to 5 ML Using Seismograms Recorded at 2.5-km Depth", *Journal of Geophysical Research: Solid Earth*, Vol. 100, No. B12, pp. 24015–24036, 1995.

14. Abercrombie, R. E., "Resolution and Uncertainties in Estimates of Earthquake Stress Drop and Energy Release", *Philosophical Transactions of the Royal Society A*, Vol. 379, No. 2196, p. 20200131, 2021.

15. Kanamori, H., "The Energy Release in Great Earthquakes", *Journal of geophysical research*, Vol. 82, No. 20, pp. 2981–2987, 1977.

16. Madariaga, R., "Implications of Stress-Drop Models of Earthquakes for the Inversion of Stress Drop from Seismic Observations", *Stress in the Earth*, pp. 301–316,

1977.

17. Amontons, G., "De la Resistance Cause'e Dans Les Machines (1)", *JOURNAL-JAPANESE SOCIETY OF TRIBOLOGISTS*, Vol. 44, pp. 229–235, 1999.

18. Godano, M., P. Bernard and P. Dublanchet, "Bayesian Inversion of Seismic Spectral Ratio for Source Scaling: Application to a Persistent Multiplet in the Western Corinth Rift", *Journal of Geophysical Research: Solid Earth*, Vol. 120, No. 11, pp. 7683–7712, 2015.

19. Boore, D. M. and J. Boatwright, "Average Body-Wave Radiation Coefficients", *Bulletin of the Seismological Society of America*, Vol. 74, No. 5, pp. 1615–1621, 1984.

20. Press, F., "Seismic Wave Attenuation in the Crust", *Journal of Geophysical Research*, Vol. 69, No. 20, pp. 4417–4418, 1964.

21. Yu, H., R. M. Harrington, H. Kao, Y. Liu, R. E. Abercrombie and B. Wang, "Well Proximity Governing Stress Drop Variation and Seismic Attenuation Associated With Hydraulic Fracturing Induced Earthquakes", *Journal of Geophysical Research: Solid Earth*, Vol. 125, No. 9, p. e2020JB020103, 2020.

22. Abercrombie, R. E. and J. R. Rice, "Can Observations of Earthquake Scaling Constrain Slip Weakening?", *Geophysical Journal International*, Vol. 162, No. 2, pp. 406–424, 2005.

23. Allmann, B. P. and P. M. Shearer, "Global Variations of Stress Drop for Moderate to Large Earthquakes", *Journal of Geophysical Research: Solid Earth*, Vol. 114, No. B1, 2009.

24. Baltay, A., S. Ide, G. Prieto and G. Beroza, "Variability in Earthquake Stress Drop and Apparent stress", *Geophysical Research Letters*, Vol. 38, No. 6, 2011.

25. Eyidoğan, H., "Jeotermal Enerji Üretimi Tuzla Fayı'nı (Çanakkale, Bababurnu) Tetiklemiş Olabilir mi?", .

26. Staszek, M., B. Orlecka-Sikora, K. Leptokaropoulos, G. Kwiatek and P. Martínez-Garzón, "Temporal Static Stress Drop Variations due to Injection Activity at The Geysers Geothermal Field, California", *Geophysical Research Letters*, Vol. 44, No. 14, pp. 7168–7176, 2017.

27. Nikurashin, M. and R. Ferrari, "Global Energy Conversion Rate From Geostrophic Flows Into Internal Lee Waves in the Deep Ocean", *Geophysical Research Letters*, Vol. 38, No. 8, 2011.

28. Kwiatek, G., F. Bulut, M. Bohnhoff and G. Dresen, "High-resolution Analysis of Seismicity Induced at Berlín Geothermal Field, El Salvador", *Geothermics*, Vol. 52, pp. 98–111, 2014.

29. Gezer, A. and T. Bekler, "6 Şubat 2017, Mw= 5.4 Ayvacık Depremi Öncesi ve Sonrası Temel Deprem Tehlike Parametrelerinin Analizi", *Journal of Advanced Research in Natural and Applied Sciences*, Vol. 7, No. 1, pp. 82–99, 6.

30. Goertz-Allmann, B. P., A. Goertz and S. Wiemer, "Stress Drop Variations of Induced Earthquakes at the Basel Geothermal Site", *Geophysical Research Letters*, Vol. 38, No. 9, 2011.

31. Shearer, P. M., R. E. Abercrombie, D. T. Trugman and W. Wang, "Comparing EGF Methods for Estimating Corner Frequency and Stress Drop from P Wave Spectra", *Journal of Geophysical Research: Solid Earth*, Vol. 124, No. 4, pp. 3966–3986, 2019.

32. Ellsworth, W. L., "Injection-Induced Earthquakes", *Science*, Vol. 341, No. 6142, p. 1225942, 2013.

33. Gibowicz, S. J., "Stress Drop and Aftershocks", *Bulletin of the Seismological So-*

ciety of America, Vol. 63, No. 4, pp. 1433–1446, 1973.

34. Bekler, T. and A. Demirci, "Preliminary Observations and Assessment of Çanakkale-Ayvacık Earthquake Activity", *Çanakkale Onsekiz Mart Üniversitesi Fen Bilimleri Enstitüsü Dergisi*, Vol. 4, No. 1, pp. 1–13, 2018.

35. Allmann, B. P. and P. M. Shearer, "Spatial and Temporal Stress Drop Variations in Small Earthquakes Near Parkfield, California", *Journal of Geophysical Research: Solid Earth*, Vol. 112, No. B4, 2007.

Table 1: The parameters of the 139 earthquakes($M_w >$ 2.8) between 2016 and 2017 .(*Cont.*)

Date	**latitude**	**longitude**	f_c**(Hz)**	M_w	$\triangle\sigma$**(MPa)**
2016.023	39.5000	25.9790	5.7	3.5496	21.6865
2016.024	39.5170	26.0030	5.46	2.9000	2.0328
2016.026	39.4980	25.9840	6.1	3.2496	9.4309
2016.028	39.5050	25.9940	8.98	2.8496	7.5732
2016.035	39.6400	26.0740	6.8	2.9663	4.9107
2016.121	39.5800	26.0440	5.4	3.0264	3.0265
2016.173	39.5100	25.9930	7.1	3.0199	6.7265
2016.180	39.4120	25.9260	1.5	3.2179	0.1257
2016.180	39.4590	25.9720	3.3	3.1232	0.9650
2016.180	39.4130	25.9140	4.0	3.7646	15.7487
2016.180	39.4320	25.9340	8.03	2.8496	5.4189
2016.181	39.3940	25.9160	3.5	3.0168	0.7972
2016.183	39.4140	25.9440	3.3	2.9983	0.6268
2016.184	39.4220	25.9390	3.6	3.1990	1.6277
2016.187	39.4240	25.9720	1.5	3.3102	0.1729
2016.204	39.4240	25.9520	7.2	2.9318	5.1744
2016.297	39.5020	26.0310	6.10	2.9000	2.8228
2016.297	39.5050	26.0460	7.60	2.8496	4.5815
2016.357	39.5340	26.1490	3.89	2.8000	0.5206
2017.002	39.5340	26.1490	7.6	3.0000	7.7020
2017.014	39.5370	26.1360	0.8	4.2474	0.6676
2017.015	39.5390	26.1080	3.6	3.4496	3.8679
2017.015	39.5400	26.1240	5.1	3.4000	9.2656
2017.018	39.5440	26.1120	3.5	3.1000	1.0626
2017.020	39.5370	26.1520	5.6	3.1330	4.8778
2017.027	39.5420	26.1220	1.3	3.1464	0.0639

2017.028	39.5440	26.1120	5.1	3.1496	3.9019
2017.030	39.6100	26.4350	5.6	3.6880	33.1687
2017.033	39.5420	26.0950	5.79	2.8000	1.7088
2017.037	39.5410	26.1170	0.5	4.9497	1.8434
2017.037	39.5310	26.1090	1.1	3.4467	0.1092
2017.037	39.5220	26.1250	3.3	2.8284	0.3486
2017.037	39.5380	26.1320	5.4	3.1984	5.4821
2017.037	39.5290	26.1030	1.8	3.8987	2.2805
2017.037	39.5430	26.1190	5.1	3.3496	7.7853
2017.037	39.5480	26.1090	5.7	3.0741	4.1970
2017.037	39.5210	26.1150	2.7	3.8000	5.4734
2017.037	39.5600	26.1260	5.1	3.5000	13.0880
2017.037	39.5300	26.1140	3.9	3.4496	4.9177
2017.037	39.5390	26.0910	3.6	3.6469	7.6458
2017.037	39.5120	26.1020	3.9	3.5412	6.7477
2017.037	39.5500	26.0790	5.1	3.3496	7.7853
2017.040	39.5470	26.0970	4.1	3.6497	11.4042
2017.040	39.5420	26.0960	5.0	3.2309	4.8688
2017.040	39.4190	26.1350	2.96	2.9000	0.3243
2017.040	39.5290	26.1640	5.18	2.8496	1.4512
2017.040	39.5150	26.1310	7.0	2.9595	5.2325
2017.040	39.5500	26.0660	7.0	3.3990	23.8758
2017.040	39.5550	26.0900	4.62	2.8496	1.0296
2017.040	39.5460	26.1210	5.15	2.9000	1.7040
2017.040	39.5330	26.0390	4.90	2.9000	1.4613
2017.040	39.5390	26.0700	4.7	3.2309	4.0440
2017.040	39.5270	26.1960	4.63	2.8496	1.0368
2017.040	39.5390	26.0580	4.14	2.9000	0.8830
2017.040	39.5430	26.1680	2.22	2.8496	0.1153

2017.040	39.5280	26.1250	5.6	3.1278	4.7910
2017.041	39.4380	26.2060	3.92	2.8000	0.5314
2017.041	39.5390	26.0620	4.2	3.3643	4.5747
2017.041	39.5430	26.0390	7.0	3.0652	7.5380
2017.041	39.5170	26.1620	1.4	4.5475	10.0878
2017.041	39.5250	26.0070	3.92	2.9000	0.7507
2017.041	39.5450	26.0510	4.14	2.9000	0.8830
2017.041	39.5320	6.1400	5.180	2.9000	1.7271
2017.041	39.5440	26.0830	5.75	2.8000	1.6784
2017.042	39.5230	26.1790	3.1	3.5412	3.3888
2017.042	39.5510	26.1360	2.2	3.9497	4.9657
2017.043	39.5380	26.0560	3.6	3.7987	12.9158
2017.043	39.5150	26.1170	0.9	4.6433	3.7311
2017.043	39.5360	26.1580	4.1	3.1937	2.3608
2017.043	39.5560	26.1160	2.4	3.6497	2.2874
2017.044	39.5230	26.1870	5.1	3.5000	13.0880
2017.045	39.5440	26.1470	3.5	3.3496	2.5163
2017.045	39.5390	26.1610	3.4	3.2000	1.3759
2017.045	39.5010	26.0630	6.8	3.0984	7.7498
2017.045	39.5400	26.0890	4.6	3.1984	3.3887
2017.046	39.5040	26.1490	6.5	3.1969	9.5116
2017.046	39.4900	26.1960	6.1	3.3289	12.4023
2017.047	39.5150	26.0590	2.5	3.9887	8.3375
2017.047	39.5160	26.0850	4.3	3.1984	2.7680
2017.047	39.5350	26.1740	4.3	3.3496	4.6663
2017.047	39.5080	26.0580	6.8	3.1984	10.9469
2017.048	39.5700	26.0760	5.1	3.1496	3.9019
2017.048	39.5320	26.1910	7.6	3.2000	15.3676
2017.050	39.5380	26.1790	5.2	3.0989	3.4716

2017.050	39.5350	26.1710	5.44	2.8496	1.6842
2017.051	39.5780	26.1730	3.13	2.8496	0.3202
2017.051	39.5120	26.0160	6.11	2.8496	2.3872
2017.052	39.5250	26.0270	5.7	3.0463	3.8128
2017.052	39.5030	26.0180	6.1	3.1496	6.6766
2017.054	39.5520	26.0970	1.9	4.0622	4.7176
2017.054	39.5000	26.2020	7.60	2.8000	3.8602
2017.054	39.4990	26.2200	6.8	3.1663	9.7981
2017.054	39.4960	26.2200	4.2	3.5321	8.1670
2017.058	39.4920	26.0650	6.1	3.1496	6.6766
2017.059	39.5070	26.0720	4.6	3.2985	4.7884
2017.060	39.4750	26.0280	3.1	3.6964	5.7923
2017.060	39.4890	26.0360	5.0	3.0663	2.7576
2017.060	39.4920	26.1320	5.50	2.8496	1.7364
2017.060	39.5050	26.0690	4.2	3.2288	2.8649
2017.060	39.4800	26.0450	10.03	2.8496	10.5464
2017.060	39.5010	26.2110	12.52	2.7495	14.5134
2017.060	39.4900	26.0640	2.5	2.9307	0.2158
2017.060	39.4960	26.0840	4.37	2.8496	0.8719
2017.060	39.5130	26.0470	3.28	2.9000	0.4396
2017.060	39.4830	26.2190	4.90	2.9000	1.4613
2017.060	39.4990	26.0200	5.78	2.9000	2.4019
2017.061	39.4820	26.0630	3.7	3.6469	8.3008
2017.061	39.5060	26.0580	4.6	3.2496	4.0442
2017.064	39.5140	26.0920	7.1	2.9983	6.2429
2017.066	39.5210	26.1740	6.0	3.1000	5.3533
2017.067	39.4920	26.1200	8.4	3.0496	12.3425
2017.068	39.5490	26.0680	5.1	2.9462	1.9327
2017.069	39.4420	26.2240	3.3	3.0984	0.8857

2017.069	39.4510	26.2250	2.7	3.1496	0.5790
2017.073	39.5280	26.1930	8.4	3.0000	10.3993
2017.074	39.5170	26.1700	5.4	3.0496	3.2790
2017.077	39.5170	26.1450	6.4	2.9933	4.4942
2017.077	39.5240	26.1630	8.0	3.1496	15.0603
2017.079	39.5270	26.1700	5.1	3.5496	15.5337
2017.079	39.5470	26.1610	1.3	4.0000	1.2190
2017.080	39.5340	26.1810	6.10	2.8496	2.3719
2017.083	39.5470	26.0980	2.4	4.1988	15.2405
2017.085	39.5020	26.1660	6.4	3.2000	9.1771
2017.087	39.5640	26.0200	7.6	3.1464	12.7704
2017.096	39.5610	26.0750	7.6	2.9983	7.6569
2017.097	39.5460	26.1790	3.8	3.4986	5.3878
2017.100	39.5370	26.2030	5.78	2.8496	2.0182
2017.100	39.5420	26.1540	4.59	2.9983	1.6882
2017.101	39.5460	26.0930	6.4	3.3985	18.2161
2017.120	39.5280	26.2080	11.87	2.9000	20.7922
2017.130	39.5280	26.1700	4.36	2.9000	1.0320
2017.140	39.5120	26.1740	11.21	2.9000	17.5263
2017.140	39.5070	26.1940	5.78	2.9000	2.4019
2017.167	39.5130	26.0660	8.49	2.9000	7.6204
2017.188	39.5270	26.1670	10.60	2.8496	12.4504
2017.201	39.5640	26.0010	9.5	3.1496	25.2194
2017.213	39.5310	26.1660	3.8	3.1464	1.5963
2017.251	39.5700	26.0470	4.6	3.2000	3.4075
2017.326	39.5910	26.1130	4.1	2.9496	1.0161